Pulsating flow in a planar diffuser upstream of automotive catalyst monoliths

Mat Yamin, A.K. , Benjamin, S.F. and Roberts, C.A.

Original citation & hyperlink:
Mat Yamin, A.K. , Benjamin, S.F. and Roberts, C.A. (2013) Pulsating flow in a planar diffuser upstream of automotive catalyst monoliths. International Journal of Heat and Fluid Flow, volume 40 : 43-53.
http://dx.doi.org/10.1016/j.ijheatfluidflow.2013.01.014

Pulsating flow in a planar diffuser upstream of automotive catalyst monoliths

A K Mat Yamin, S F Benjamin*, C A Roberts

Faculty of Engineering and Computing
Coventry University
Priory St
Coventry CV1 5FB
UK

s.benjamin@coventry.ac.uk
Tel +44 (0)2476 888362

*Corresponding author

Abstract

The flow distribution across automotive exhaust catalysts has a significant effect on their conversion efficiency. The exhaust gas is pulsating and flow distribution is a function of engine operating condition, namely speed (frequency) and load (flow rate). This study reports on flow measurements made across catalyst monoliths placed downstream of a wide-angled planar diffuser presented with pulsating flow. Cycle-resolved Particle Image Velocimetry (PIV) measurements were made in the diffuser and hot wire anemometry (HWA) downstream of the monoliths. The ratio of pulse period to residence time within the diffuser (defined as the J factor) characterises the flow distribution. During acceleration the flow remained attached to the diffuser walls for some distance before separating near the diffuser inlet later in the cycle. Two cases with J~3.5 resulted in very similar flow fields with the flow able to reattach downstream of the separation bubbles. With J=6.8 separation occurred earlier with the flow field resembling, at the time of deceleration, the steady flow field. Increasing J from 3.5 to 6.8 resulted in greater flow maldistribution within the monoliths; steady flow producing the highest maldistribution in all cases for the same Re.

Keywords: pulsating flow; diffuser; exhaust catalysts

1 Introduction

Catalysts are used extensively in the automotive industry to reduce toxic pollutants from vehicle exhausts. They are usually ceramic monolith structures, comprised of several thousand channels, often of square cross-section, of small hydraulic diameter (~ 1mm). The catalyst materials (precious metals) are embedded in a thin washcoat which is applied to the channel walls thus providing a high surface area on which exhaust pollutants can react. The size and shape of the monolith depends on vehicle size and packaging constraints. Typically a monolith for a passenger vehicle would have a circular or oval cross-section of diameter and length ~100-150 mm with cell densities normally varying between 31 and 140 cells/cm^2. Space constraints dictate that wide-angled diffusers are employed to connect the exhaust pipe to the front face of the catalysts. This leads to flow separation at the inlet to the diffuser and a non-uniform distribution of flow into the channels. Fig.1 shows a typical assembly featuring a monolith located downstream of a wide-angled diffuser along with a representation of the flow field within the diffuser with steady flow. The exhaust stream is shown separating at the diffuser inlet forming a jet which traverses the body of the diffuser before spreading rapidly as it approaches the monolith. Part of the flow recirculates and part enters the monolith. Flow separation causes maldistributed flow and non uniform heat flux within the monolith leading to premature deactivation of the catalyst in areas of high flow. Maldistributed flow in general will cause a reduction in conversion efficiency, an increase in system pressure loss and poor utilisation of the catalyst. Many studies have been performed over the years to investigate the effect of system geometry on flow distribution and converter performance; for example Howitt and Sekella (1974), Zygourakis (1989) and Weltens et al (1993). Indeed the degree of flow uniformity across the monolith is often used as an indicator for the acceptability of a particular design with various indices being used to quantify this, e.g. Weltens et al (1993), Benjamin et al (2002). The system geometry is often complex and the exhaust is pulsating and so predicting or measuring the flow across the monolith presents serious challenges.

To simplify the situation many studies have been conducted under the assumption that the flow can be considered as non-pulsating or steady. This approximates the situation where the catalyst is located at some considerable distance downstream of the exhaust ports, so-called under-body designs. Under such conditions measurements can be made using steady flow rigs which permit a more comprehensive analysis of the flow field within the diffuser and the flow distribution across the monolith. Because the flow is unidirectional as it exits

the channels hot wire anemometry (HWA) or pitot traverse at the rear of the monolith can be used to quantify flow maldistribution. Such studies can provide useful correlations between flow distribution within the monolith, system geometry and monolith resistance (Benjamin et al (1996)). PIV measurements in the upstream diffuser have also been reported by several groups for steady flow. Shuai et al (2001) examined diffuser and monolith designs and compared measurements with computational fluid dynamic (CFD) predictions. In a recent study Turner et al (2011) similarly studied the flow field upstream of a diesel particulate filter. Ilgner et al (2001), made PIV measurements upstream of an auto-thermal gas reformer but significant image distortion due to wall curvature restricted the field of view where reliable data could be obtained. Using a planar diffuser optical distortion was minimised by Quadri et al (2009a). By comparing the upstream flow field (PIV) with that measured downstream of the monolith using HWA it was demonstrated that the monolith radically redistributes the flow as it enters the channels.

Stricter emission legislation has meant catalysts are now located closer to the engine in order to reduce light-off times; so called close-coupled systems. For such configurations the flow is highly pulsating and a steady flow analysis is inappropriate. Pulsating flows through expanders have been the subject of limited studies. Budwig and Tavoularis (1995) measured the flow field in an open axisymmetric sudden expansion using a two-component LDV system under steady and pulsatile flows albeit at low Re (~120) and frequency (~0.2Hz). They found that the pulsatile flow recirculation zone lengths revealed a dramatic departure from quasi-steady prediction; the instantaneous lengths correlating with the acceleration of the flow rather than the instantaneous Re. Under more representative flow conditions oscillating and pulsating PIV measurements have been obtained in open planar diffusers, Smith and King (2007) and King and Smith (2011). Their flow rig is capable of velocity oscillation amplitudes up to 50 m/s at frequencies of 7 to 120 Hz and steady flows up to 40 m/s. These are flow conditions more closely representative of engine exhausts. In Smith and King (2007) PIV measurements were made on diffusers with included angles up to 30^o. With oscillating flow, during the acceleration part of the cycle, the flow remained attached in spite of very large adverse pressure gradients. During deceleration the flow was more prone to separation. Oscillating and pulsating flows at the same point of the cycle (start of deceleration) were also compared. For both cases flow is shown separating near the diffuser inlet but is able to reattach in the former case. In a recent study King and Smith (2011) they reported on further observations made under oscillating conditions. Separation was found to begin high in the diffuser and propagated downward; the flow was able to remain attached further into the diffuser with larger Re, small displacement amplitudes and smaller diffuser angles. They also showed that the extent of flow separation grows with a non-dimensional displacement amplitude, a function of the maximum velocity and pulsation frequency. Conditions associated with exhaust after-treatment systems are however somewhat different in several key aspects; the flow is essentially pulsating and the proximity of the monolith will have a significant effect on flow development in the diffuser. Such studies that have been performed for these systems have been made using either rigs or running engines e.g. Hwang et al (1995), Bressler et al (1996), Zhao et al (1997), Park et al (1998) and Benjamin et al (2006). Whilst of great practical importance they most often feature "production type" exhausts which are geometrically complex providing limited access for flow measurements. A number of pulsating flow rig studies has also been reported using simpler axisymmetric geometries. Benjamin et al (2001) measured the effect of flow pulsations on the flow distribution within ceramic contoured monoliths by measuring the cycle-averaged flow distribution at the exit to the monoliths using HWA. Contoured monoliths were shown to be less sensitive to changes in flow rate and pulsation frequency when compared to a standard monolith. Liu et al (2003) investigated the effect of pulse shapes. Pulses with higher peak/mean ratio produced less maldistributed flow at all frequencies. Benjamin et al (2002) studied the effect of pulse frequency (16-100 Hz) and Re ($2x10^4$-$8x10^4$) on the flow distribution within monoliths of different lengths with 60^o and 180^o diffusers. Both cycle-averaged and phase-averaged velocity profiles were presented. Flow maldistribution within the monolith was defined as a non-uniformity index ψ; the mass weighted standard deviation of the axial velocity across the monolith normalised to the average velocity. This index was shown to be determined by a non-dimensional parameter J (reciprocal of the Strouhal number) defined as the ratio of pulse period to residence time within the diffuser; as J increased ψ also increased. J is similar to the non-dimensional displacement amplitude introduced by King and Barton (2011). Persoons et al (2003) found a similar correlation between their measure of flow uniformity and a scavenging ratio S (defined in a very similar way to J) for the case of a more complex system geometry.

Whilst these studies were able to derive useful correlations between flow maldistribution and system parameters it is often difficult to interpret the findings in terms of processes within the diffuser itself. This paper begins to address this issue by presenting measurements of the flow field both within a diffuser and downstream of the monolith in the presence of pulsating flow. The first objective of the study was to provide insight into the development of the pulsating flow field for a relatively simple yet representative after-treatment configuration. A second objective was to provide experimental data against which computational fluid dynamics (CFD) predictions could be assessed. Both objectives are seen as useful starting points before consideration of more complex, production-type systems.

2 Experimental Method

Experiments were conducted under isothermal conditions at ambient temperature and similarity with hot engine exhaust was based on Re. For this study a planar wide-angled diffuser was chosen to enable maximum optical access and simplify measurement as the flow is approximately two-dimensional. Whilst idealised it is expected to show many of the flow features common to more complex systems and, to a first approximation, may be thought of as representative of oval or elliptical designs. Fig. 2 shows a schematic of the rig. It was supplied with compressed air via a plenum (2) incorporating a flow straightener (3) placed upstream of an axisymmetric nozzle (4). Pulsations are generated by a pulse generator (5) placed downstream of the nozzle as used in previous studies (Benjamin et al 2002). A 12 mm aluminium housing contains a cast iron plate with four regularly spaced openings. A DC motor rotates the plate which periodically interrupts the flow. Timing signals and rotational speed are obtained from an optical-electrical transducer (+-5V output voltage) within the rotor assembly. Non-pulsating flow was achieved by fixing the rotor in one of its fully open positions. A flow straightener (6) was placed downstream of the rotor and a resonator box (7) was installed in order to shape the pulses. The plenum (8) mixes seeding particles supplied by a particle generator (9); the flow straightener (10) in the plenum minimizes any swirl components. The rectangular nozzle (11) produces a uniform velocity profile into the planar diffuser (12). Thus well-defined inlet boundary conditions are generated suitable for CFD modelling. The diffuser has inlet dimensions 24 x 96 mm, a total included angle of approximately 60^o, length 48 mm and an outlet 78 x 96 mm. The walls of the diffuser were made from crown glass for maximum optical access. Unwashcoated cordierite monoliths (13) of length 27 mm or 100 mm were positioned downstream of the diffuser. The monoliths had channel hydraulic diameter of 1.12 mm, a nominal cell density of 62 cells/cm^2 and a porosity of 0.77. An outlet sleeve (14) of length 50 mm was used to minimise disturbance by surrounding air when making HWA measurements at the exit from the monolith.

A TSI IFA 300 constant temperature hot-wire anemometry (HWA) system was used to measure the axial velocity within the inlet to the diffuser and at the exit of the monolith. The probes were 5 µm platinum-plated tungsten wires (Dantec 55 P11) and were calibrated using a fully automatic TSI 1129 calibration rig. A 1MHz 4 channel 12 bit A/D converter was used to convert the IFA output voltage (within +- 5 V) to a digital signal, which was then processed by the ThermalPro software to compute the instantaneous and time-averaged velocity. The signals were channelled into the A/D board of the IFA 300 system. Signals from the pulse generator and HWA probe were logged simultaneously. Using the timing signal HWA velocity profiles were derived by phase-averaging over 50 cycles. A sampling size of 2048 points was used with the sampling rate of 2 kHz for flow pulsating frequencies of 50Hz and 4 kHz for 100Hz to obtain 40 data points per cycle.

Measurements inside the diffuser were conducted using a TSI PIV system. The flow was seeded by a six-jet atomizer at 25 psi to produce ~ 0.6 µm diameter droplets of olive oil. A cylindrical lens of -25 mm focal length was combined with a spherical lens of 500 mm to transform the circular beam from a 120 mJ solid-state Nd:YAG laser into an approximately 1mm thickness light-sheet at a stand-off distance of 0.5 m to illuminate the seeded flow. A 4-megapixel CCD camera with a resolution of 2048 x 2048 pixel (1 pixel = 7.4 µm) was used to capture the flow field. The camera coupled with a 105 mm lens was placed 0.8 m from the measurement plane to cover a 80 mm x 60 mm field of view resulting in a magnification factor of 0.155. To avoid pixel locking, the f number of 11 was used to achieve a particle image diameter above 2 pixels (Rafell and Willert(1998)). The PIV data were processed using INSIGHT-3G software and plotted using Techplot 11. The recursive Nyquist method with an initial grid size of 64 x 64 and a final grid of 32 x 32 pixels yielded 95% of valid vectors in each field and vector resolution of 0.76 mm. Phase-averaged measurements over 100 cycles were performed using the signal from the pulse generator to trigger measurements at specified points in the cycle.

3 Results

3.1 Steady flow

The results from steady flow measurements are reported first. Fig. 3 shows velocity profiles across both planes at the centre of the nozzle outlet. Profiles are acceptably uniform and the flow in the diffuser would be expected to be symmetric and two-dimensional. Fig. 4 shows normalized velocity and vorticity maps as the average of 100 consecutive fields for Re= $4.3x10^4$ and monolith length 27 mm. The flow field is essentially symmetric. Some data loss occurred at the sealed joints at the inlet and outlet of the diffuser, in the latter case up to a distance of 2.5 mm from the front face of the monolith. However the bulk of the flow field in the diffuser is captured. Flow separation at the inlet results in a planar jet that traverses the diffuser. On approaching the

monolith it spreads rapidly, part entering the monolith channels, part reversing to feed the two large recirculating vortices. This vortex-pair confines and narrows the jet resulting in non-dimensional velocities greater than 1 near the diffuser inlet. Vorticity generated within the shear layer between the jet and the surrounding fluid is convected downstream and diffused within the two large recirculating vortices. The central region of the jet has low vorticity corresponding to its potential core.

Fig. 5 shows contours of normalized velocity for two Re and both monoliths. Re is defined as $U_{in}d_h/\nu$ where U_{in} is the mean velocity at the diffuser inlet, d_h the hydraulic diameter of the nozzle (38.4 mm) and ν the kinematic viscosity. The shear layers at the sides of the jet are clearly shown as are the saddle-shape profiles in its potential core; similar features have been observed by Quadri et. al. (2009a). With lower Re and greater downstream resistance (longer monolith) the flow profiles near the front face of the monolith are flattened. PIV velocity profiles across the diffuser at a distance of 2.5 mm from the front face of the monoliths are shown in fig.6. This again illustrates profile flattening with the lower Re and longer monolith. Fig. 6 also shows the HWA profiles obtained 40 mm downstream of the monoliths; at this distance jets exiting neighbouring channels mix sufficiently to provide relatively smooth profiles (Benjamin et. al. 1996). These profiles are representative of the flow distribution within the monolith as the flow essentially remains uni-directional as it exits the channels. Again flatter profiles within the monolith are observed for the lower Re and with the longer monolith. Similar results have been reported for axisymmetric systems (Benjamin et al 1996). Of particular note is the significant difference in profile shape between the PIV and HWA. The flow distribution changes radically between 2.5 mm and the front face of the monolith. This flow restructuring is complex and is determined by the losses associated with the flow entering the channels plus viscous losses within the channels themselves. At the jet centre-line, where velocities are greatest, the latter dominate and a radial pressure gradient is formed across the front face of the monolith thus spreading the jet. Consequently, away from the centre-line, fluid approaches the channels obliquely at an angle of incidence which increases with radial distance. Oblique entry losses are very significant at high incidence and can exceed viscous losses ((Quadri et al (2009b), Persoons et al (2008)) thus forcing more flow towards the walls. As it approaches the wall it decelerates and the local pressure increases, which encourages flow through the outer channels. The net result is the formation of the secondary velocity peaks within the monolith about 10 mm from the wall.

3.2 Pulsating Flow

PIV and HWA measurements were obtained for cases shown in table 1. Measurements were obtained for Re = $2.2\text{x}10^4$ and ~$4.2\text{x}10^4$ and at 50 and 100 Hz with monoliths of length L=27 and 100 mm. The space velocity (inverse of the residence time within the monolith) for the PIV experiments is also shown as it is commonly used for reactor flows. Flow regimes may be characterised by a parameter J defined as the ratio of pulse period to residence time in the diffuser. J is given as $U_{in}/L_d f$, where U_{in} is the mean inlet velocity, f pulse frequency and L_d, the length of the diffuser. The cases with J~ 3.5 correspond to Re = $2.2\text{x}10^4$, f = 50 Hz and Re ~ $4.2\text{x}10^4$, f = 100 Hz. The cases for J=6.8 corresponds to Re ~ $4.2\text{x}10^4$, f = 50 Hz. As discussed in section 1 with axisymmetric assemblies flow maldistribution within the monolith correlated with J (Benjamin et al 2002). Steady flow may be considered as the limiting case as J approaches infinity, i.e. pulse period becomes infinitely long.

Fig. 7 shows pulse shapes measured by HWA at the centre of the inlet duct. Whilst some variation exists between the two frequencies they exhibit similar peak/mean ratios and are largely independent of Re and monolith length. An example of velocity profiles at the inlet to the diffuser is shown in fig. 8. The profiles were obtained as phase-averages at various non-dimensional times (t/T) throughout the cycle. Profiles are flat as for the steady flow cases.

3.2.1 Flow field for J=6.8 (Case 3).

Fig. 9 shows the normalised velocity and vorticity fields for J=6.8 with the 27 mm monolith. The corresponding fields for 100mm were similar in many respects and so are not reported here. Fig.7 shows deceleration occurs from t/T=0.6 to 1.0. At the time of maximum inlet velocity, t/T=0.6, the flow field is similar to that for steady flow. The inlet inertia at this time is sufficient to cause separation near the inlet. The resulting jet traverses the diffuser, rapidly spreading near the front of the monolith and either entering the channels or recirculating within the diffuser. High vorticity is generated in the shear layer at the edges of the jet which is subsequently mixed within the separation bubble. The central region of the jet has low vorticity corresponding to its potential core. As the flow decelerates the vortex pair is able to “squeeze” the jet core; this is especially noticeable near the

inlet at t/T=1.0. During deceleration vorticity generation at the inlet is reduced and is also dissipating within the dominant vortex structures. At t/T=0.8, the inlet velocity is approximately equal to the cycle-averaged value. Hence the flow field can be compared with that for steady flow as shown in fig. 10 where velocity contour maps are illustrated for 27 and 100 mm monoliths. The contours are similar in many respects. The larger resistance of the 100 mm monolith reduces the velocity in the central region and causes greater spreading of the jet for both steady and pulsating flow. The recirculating vortices for pulsating flow are evidently too transient in nature to produce the saddle shapes featured with steady flow within the main body of the diffuser.

The flow accelerates from t/T =0.1 to 0.5. Fig. 9 shows the recirculation regions from the previous cycle still residing in the diffuser at t/T=0.1. From t/T=0.1- 0.2, the low inlet inertia allows the flow to stay attached for some distance along the wall. As the flow expands it transports the residual vortex structures from the previous cycle through the diffuser. At t/T=0.2, the inlet velocity is again approximately equal to the cycle-averaged value but the flow field is quite different from that at t/T=0.8. From t/T=0.3-0.5, as inlet inertia increases, the flow detaches forming separation bubbles illustrated by the growing region of vorticity. The flow is able to reattach behind the bubbles resulting in relatively uniform flow at the monolith as the residual vortex has now been pushed out of the diffuser. The net effect is that the time-averaged flow distribution at the front face of the monolith is improved compared with that for steady flow i.e. pulsations have reduced flow maldistribution. From t/T=0.5 the flow again begins to resemble that for steady flow as the accelerating inlet jet approaches the monolith.

3.2.2 Flow field comparison at 50 Hz with varying J (Cases 1 and 3).

Fig.11 compares side-by-side the normalised velocity vector and vorticity fields at 50Hz for Re= $2.2x10^4$ and $4.2x10^4$, corresponding to J=3.6 and 6.8 respectively. The flow field for J=3.6 exhibits features similar to those discussed earlier for J=6.8. During acceleration, the flow initially remains attached pushing the residual vortex from the previous cycle out of the diffuser. Separation occurs at t/T=0.4 and the inlet jet and its associated vortex structure begin to develop within the diffuser. During deceleration the recirculating zone increases in size effectively squeezing the jet as it loses momentum (t/T=0.8). However significant differences are observed at the lower Re. The reduced inlet inertia during acceleration is less effective at removing the residual vortices; at t/T =0.3, for example, they have already been eliminated at the higher Re. Flow separation occurs later and so there is a reduction in size of the separation bubbles at equivalent times. As a consequence, during deceleration (t/T=0.6, 0.7), the flow is able to reattach downstream of the bubbles resulting in a flatter distribution at the monolith at the lower J value.

3.2.3 Flow field comparison at Re 4.2 $x10^4$ with varying J (Cases 3 and 5).

Fig.12 compares side-by-side normalised velocity vector and vorticity fields at 100Hz and 50 Hz for Re= $4.2x10^4$, corresponding to J= 3.4 and 6.8 respectively. Flow development at the higher frequency is very similar to that observed for J= 3.6 in fig.11 i.e. longer retention of residual vorticity from the previous cycle, later separation during acceleration and smaller recirculation bubbles. It would appear that at the higher frequency the flow does not have sufficient time to establish the inertia dominated flow regimes associated with lower frequencies and/or higher Re.

3.3 Flow maldistribution in the monolith

Fig. 13 compares the cycle-averaged pulsating flow distributions downstream of the 27 and 100 mm monoliths with those for steady flow. Such a comparison is useful for assessing the adequacy of deducing flow maldistribution in engine flows based on a steady flow analysis. For a given monolith profiles for J ~ 3.5 are very similar whereas the flow maldistribution is greater with J=6.8; findings which are consistent with the flow fields obtained upstream in the diffuser. For a given Re the flow maldistribution is highest with steady flow (J infinite), the differences being more pronounced for the shorter monolith. For the longer monolith the distributions are flatter for all cases as a consequence of the greater downstream resistance. Hence with higher resistance the effect of pulsations will have a reduced impact on the mean flow maldistribution.

In section 3.1 flow restructuring at the front face of the monolith was discussed for the case of steady flow. It is anticipated that similar restructuring will occur for the case of pulsating flow. This is clear from fig. 14 which compares the PIV cycle-averaged velocity profiles just upstream of both monoliths to those observed downstream for J=6.8. As for the case of steady flow it is clear that considerable flow restructuring occurs within 2.5 mm of the front face of the monolith.

The effect of pulsations on the flow distribution across automotive catalysts can therefore be significant. Clearly the functional relationship between flow uniformity and the J-factor will depend on engine type and exhaust after-treatment geometry. Although the study has been undertaken for an ideal planar geometry the expectation is that similar functional relationships would be equally valid for more practical configurations. Indeed this has already been established for conical diffuser by the present authors Benjamin et al (2002) and for the case of more complex geometries Persoons et al (2003). For situations with high flow, low engine speed and after-treatment systems with short monoliths (e.g. close-coupled systems) flow maldistribution will be increased.

4 Conclusions

PIV studies have been performed in a planar wide-angled diffuser placed upstream of automotive exhaust monoliths. Studies were undertaken at frequencies of 50 and 100 Hz for Re = $2.2x10^4$ and $4.2x10^4$ and compared to steady flow measurements. The spatial and temporal velocity distribution at the exit of the monoliths was also recorded using hot wire anemometry (HWA). The ratio of pulse period to residence time within the diffuser (J factor) was used to characterise the flow. Measurements were obtained for J~3.5 and 6.8.

With steady flow, separation occurred at the inlet to the diffuser for both Re resulting in a planar jet that traversed the diffuser. On approaching the monolith it spread rapidly, part entering the monolith channels, part reversing to feed the two large recirculating vortices. Significant flow restructuring occurs in the diffuser just upstream of the monolith as the flow enters the monolith channels.

With pulsations the flow field varied throughout the cycle. Initially, as the flow accelerated, it remained attached to the diffuser walls for some distance. Separation bubbles then formed near the diffuser inlet resulting in the development, later in the cycle, of two large recirculating vortices. These vortices occupied the diffuser volume at the end of the pulse before being transported out during the subsequent cycle. Flow separation occurred earlier for J= 6.8 with larger vortex structures dominating the diffuser. The flow field at the beginning of the deceleration phase resembled that under steady flow conditions. Two cases with J~3.5 resulted in very similar flow fields. In each, the flow was able to reattach downstream of the separation bubbles during part of the cycle thus presenting more uniform flow to the monolith. Low Re and high frequency pulses (low J) do not permit the flow to establish sufficient inertia to provide the fully separated flow regimes observed under steady flow conditions and so result in flatter profiles within the monolith. Increasing J from ~3.5 to 6.8 resulted in greater flow maldistribution in the monolith; steady flow produced the highest maldistribution at the same Re. Increasing monolith resistance flattens the flow field just upstream and within the monolith for both steady and pulsating flows.

Acknowledgement.

Financial support for A. K. Mat Yamin was received from Universiti Teknikal Malaysia Melaka (UTeM), Malaysia.

References

Benjamin, S.F., Clarkson, R.J., Haimad, N., Girgis, N.S.,1996. An experimental and predictive study of the flow in axisymmetric automotive exhaust catalyst systems. SAE Tran. J. Fuels Lubricants. 105, (4), 1008-1019.

Benjamin, S.F., Roberts, C.A., Wollin, J., 2001. A study of the effect of flow pulsations on the flow edistribution within ceramic contoured catalyst substrates. SAE Tran. J. Fuels Lubricants. 110, (4), 1380-1387.

Benjamin, S.F., Roberts, C.A., Wollin, J., 2002. A study of pulsating flow in automotive catalyst systems. Exp Fluids. 33, 629-639.

Benjamin, S.F., Disdale, W., Liu, Z., Roberts, C.A., Zhao, H., 2006. Velocity predictions from a coupled 1D/3D CFD simulation compared with measurements in the catalyst system of a firing engine. Int. J. Engine Res. 7, (1) 29-40.

Bressler, H., Rammoser, D., Neumaier, H., Terres, F., 1996. Experimental and predictive investigation of a closed coupled catalytic converter with pulsating flow. SAE paper 960564. SP-1173. SAE International Warrendale,PA.

Budwig, R., Tavoularis, S. 1995. Steady and Pulsatile flows through an axisymmetric sudden expansion. FED-Vol. 216, Unsteady Flows-ASME 1995.

Howitt, J.S., Sekella, T.C., 1974. Flow effects in monolithic honeycomb catalytic converters. SAE Paper 740244

Hwang, K., Lee, K., Mueller, J., Stuecken, T., Schock, H.J., Lee, J-C., 1995. Dynamic flow study in a catalytic converter using laser doppler velocimetry and high speed flow visualisation. SAE paper 950786. SP-1094 Global Emission experiences:processes, measurements, and substrates. SAE International Warrendale, PA. 169-186.

Ilgner, F., Nau, M., Harndorf, H., Benninger, K., Schiessl, R., Maas, U., Dreizler, A., 2001. Analysis of flow patterns inside an autothermal gasoline reformer. SAE Paper 2001-01-1917.

King, C.V., Smith, B.L., 2011. Oscillating flow in a 2D diffuser. Exp Fluids. 51, (6) 1577-1590.

Liu, Z., Benjamin, S.F., Roberts, C.A., 2003. Pulsating flow maldistribution within an axisymmetric catalytic converter-flow rig experiment and transient CFD simulation. SAE 2003-01-3070, SP-1801 SAE International Warrendale, PA.

Park, S-B., Kim, H-S., Cho, K-M., Kim, W-T., 1998. An experimental and computational study of flow characteristics in exhaust manifold and CCC (closed coupled catalyst). SAE paper 980128.

Persoons, T., Van den Bulk, E., Fausto, S. 2003. Study of pulsating flow in a close-coupled catalyst manifold using phase-locked hot-wire anemometry. Exp Fluids. 36, (2) 217-232.

Persoons, T., Vanierschot, M, Van den Bulck, E., 2008. Oblique inlet pressure loss for swirling flow entering a catalyst substrate. Exp. Therm. Fluid Sci. 32, 1223-1231.

Quadri, S.S., Benjamin, S.F., Roberts, C.A., 2009a. Flow measurements across an automotive catalyst monolith situated downstream of a planar wide-angled diffuser. Proc IMechE 224, Part C, J. Mechanical Engineering Science. 321-328.

Quadri, S.S., Benjamin, S.F., Roberts, C., 2009b. An experimental investigation of oblique entry pressure losses in automotive catalytic converters . Proc IMechE. 223, (11), Part C, J. Mechanical Engineering Science,2561-2569.

Rafell, M., Willert, C, Kompenhaus, J., 1998. Particle image velocimetry, Springer, Berlin

Shuai, S-J., Wang, J-X., Dong, Q-L., Zhang, R-J., 2001. PIV measurement and numerical simulation of flows in automotive catalytic converters. SAE paper 2001-01-3494.

Smith, B.L., King, C.V., 2007. Time-resolved PIV and pressure measurements of oscillating and pulsating flow in a rapid expansion. FEDSM2007-37257 Proceeding of FEDSM2007 5th Joint ASME/JSME Fluids Engineering Conference San Diego, USA.

Turner, C., Thornhill, D, McCullough, G., 2011. Comparison of experimental PIV data and CFD simulations for flow in a Diesel particulate filter inlet diffuser. SAE paper 2011-01-1241.

Weltens, H., Bressler, H., Terres, F., Neumaier, H., Rammoser, D., 1993. Optimisation of catalytic converter gas flow distribution by CFD predictions SAE paper 930780.

Zhao, F-Q., Bai, L., Liu, Y., Chue T-H, Lai, M-C., 1997. Transient flow characteristics inside the catalytic converter of a firing gasoline engine. SAE paper 971014. Reprinted from SP-1248: Issues in Emissions Control Technology, SAE International, Warrendale, PA, 175 – 188.

Zygourakis, K., 1989. Transient operation of monolith catalytic converters: a two-dimensional reactor model and the effects of radially non-uniform flow distributions Chem. Engng. Sci. 44 (9) 2075-2086.

Figures and Table

Fig 1 Schematic showing catalyst configuration comprising a monolith in an exhaust system, catalyst channels and flow separation in the diffuser

Fig 2 Schematic of the rig

Fig 3 Velocity profiles across the centre of the nozzle exit measured across both planes with HWA

Fig 4 Steady flow normalised vector and vorticity fields. Re = 4.3 x 10^4, monolith length L = 27 mm, u axial and v transverse velocities, U_1 inlet mean velocity, ω vorticity and L_d length of diffuser

Fig 5 Contours of normalised velocities with steady flow (a) Re = 2.3 x 10^4 (left), Re = 6.2 x 10^4 (right), L = 27 mm (b) Re = 6.2 x 10^4, L = 27 mm (left), 100 mm (right)

Fig 6 Steady flow. Normalised axial velocity distributions 2.5 mm upstream (PIV) and 40 mm downstream (HWA); u axial velocity, U_2 mean velocity downstream of the monolith

Fig 7 Inlet pulse shapes observed at centre of the nozzle exit for (a) 100 Hz and (b) 50 Hz, t is the time, T pulse period, u phase-averaged velocity, u_{Mean} cycle-averaged velocity

Fig. 8 Phase-averaged velocity profiles across centre of the nozzle exit (f = 50 Hz, Re = 2.1 x 10^4, L = 27 mm)

Fig. 9 Normalised phase-averaged velocity vector and vorticity fields for Case 3 at J = 6.8 (Re = 4.2x10^4, f =50 Hz, L = 27mm). Fields are normalised by the cycle-averaged mean inlet velocity

Fig 10 Normalised velocity contours at Re ~ 4.2 x 10^4 (a) t/T = 0.8, Case (3), f = 50 Hz, L = 27 mm (b) Steady flow, L = 27 mm (c) t/T = 0.8, Case (4), f = 50 Hz, L = 100 mm (d) Steady flow, L = 100 mm. In (a) and (c) phase-averaged velocities are normalised by the cycle-averaged mean inlet velocity

Fig 11 Normalised phased averaged velocity and vorticity fields for Case 1 (J = 3.6, Re = 2.2 x 10^4, 50 Hz) and Case 3 (J = 6.8, Re = 4.2 x 10^4, 50 Hz) for L = 27 mm. Fields are normalised by the cycle-averaged mean inlet velocity

Fig 12 Normalised phase-averaged velocity and vorticity fields for Case 3 (J = 6.8, Re = 4.2 x 10^4, 50 Hz) and Case 5 (J = 3.4, Re = 4.2 x 10^4, 100 Hz) for L = 27 mm. Fields are normalised by the cycle-averaged mean inlet velocity

Fig 13 Steady flow and cycle-averaged velocity profiles at the monolith exit. Velocities are normalised by the cycle-averaged mean velocity downstream of the monolith

Fig 14 Cycle-averaged velocity profiles measured 2.5 mm upstream (PIV) and 40 mm downstream (HWA) for Re ~ 4.2 x 10^4, f = 50 Hz, J = 6.8 for L = 27 mm and 100 mm (Cases 3 and 4). Velocities are normalised by the cycle-averaged mean velocity downstream of the monolith

Table 1 Test cases

Table 1 Test cases

PIV measurements						
Case	1	2	3	4	5	6
L(mm)	27	100	27	100	27	100
Space velocity (hr^{-1})	$2.6x10^5$	$6.7x10^4$	$4.9x10^5$	$1.3x10^5$	$4.9x10^5$	$1.3x10^5$
f (Hz)	50	50	50	50	100	100
Re $x10^{-4}$	2.24	2.25	4.19	4.19	4.16	4.21
J(-)	3.6	3.6	6.8	6.8	3.4	3.4
HWA measurements						
Re $x10^{-4}$	2.18	2.19	4.10	4.12	4.09	4.12
J (-)	3.5	3.6	6.8	6.8	3.4	3.4

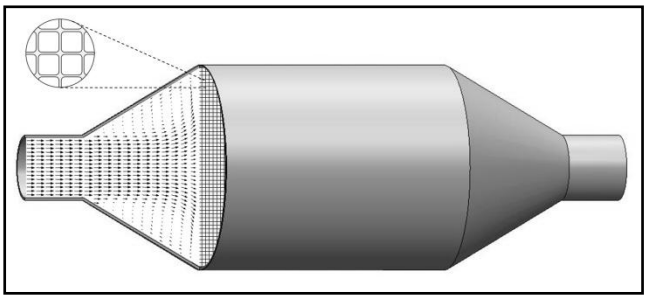

Fig. 1 Schematic showing catalyst configuration comprising a monolith in an exhaust system, catalyst channels and flow separation in the diffuser

Figure

Click here to download Figure: Figure 2 Int J of Heat and Fluid Flow 22 March 2012.docx

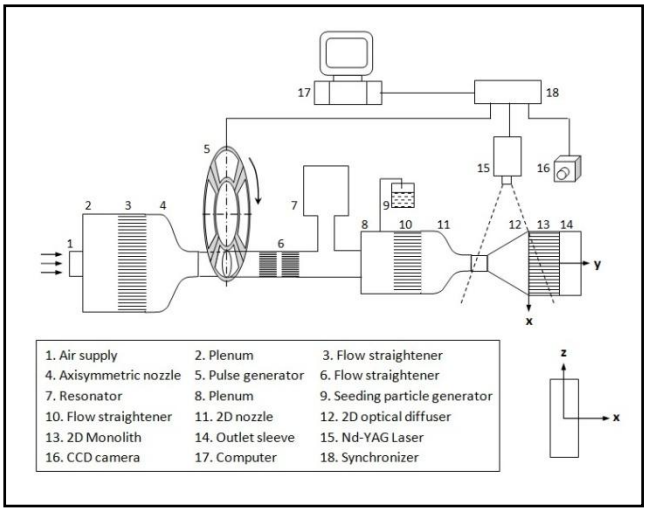

Fig. 2 Schematic of the rig

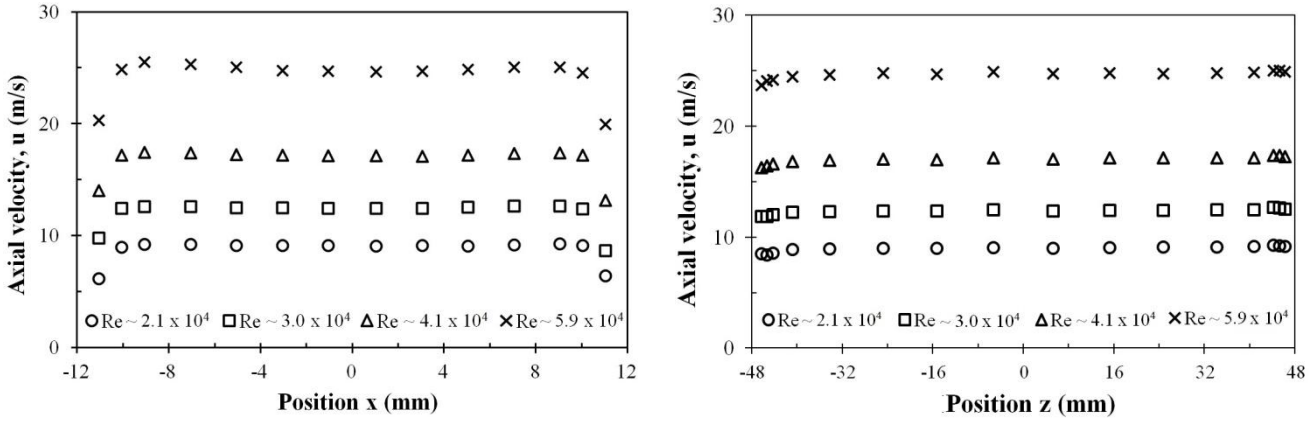

Fig. 3 Velocity profiles across the centre of the nozzle exit measured across both planes with HWA

Figure
Click here to download Figure: Figure 4 Int J of Heat and Fluid Flow 22 March 2012.docx

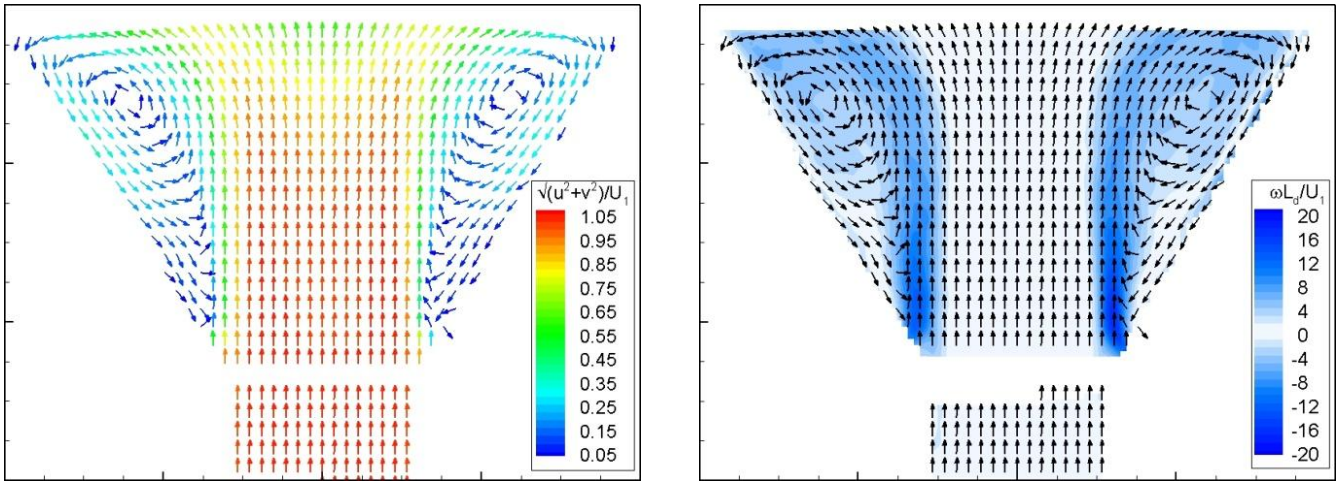

Fig. 4 Steady flow normalised vector and vorticity fields. Re = 4.3 x 10^4, monolith length L = 27 mm, u axial and v transverse velocities, U_1 inlet mean velocity, ω vorticity and L_d length of diffuser

Figure
Click here to download Figure: Figure 5 Int J of Heat and Fluid Flow 22 March 2012.docx

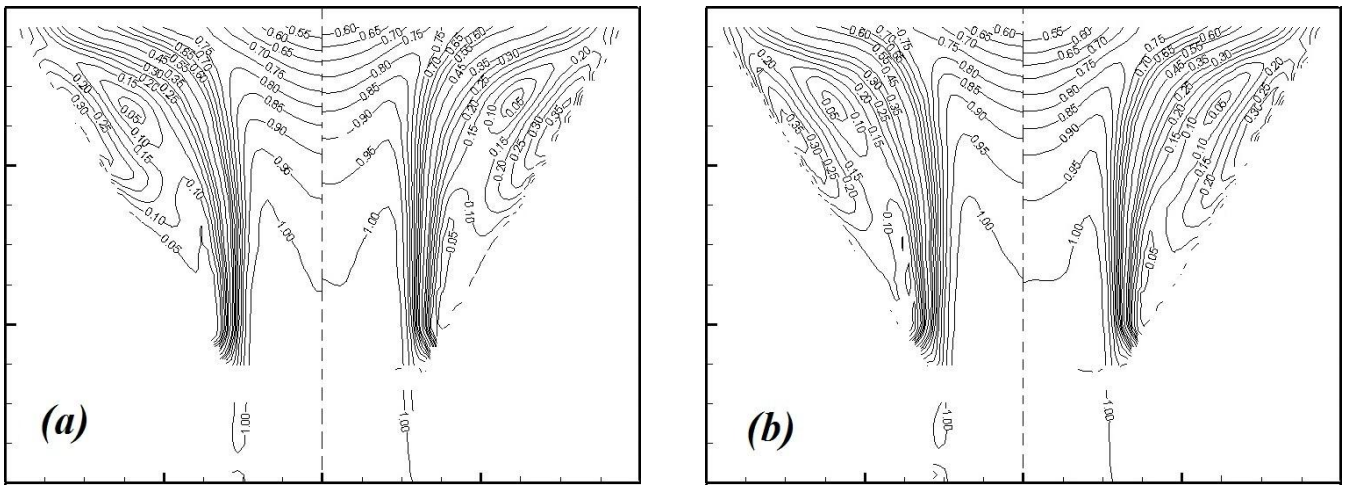

Fig. 5 Contours of normalised velocities with steady flow (a) Re = 2.3 x 10^4 (left), Re = 6.2 x 10^4 (right), L = 27 mm (b) Re = 6.2 x 10^4, L = 27 mm (left), 100 mm (right)

Figure
Click here to download Figure: Figure 6 Int J of Heat and Fluid Flow 22 March 2012.docx

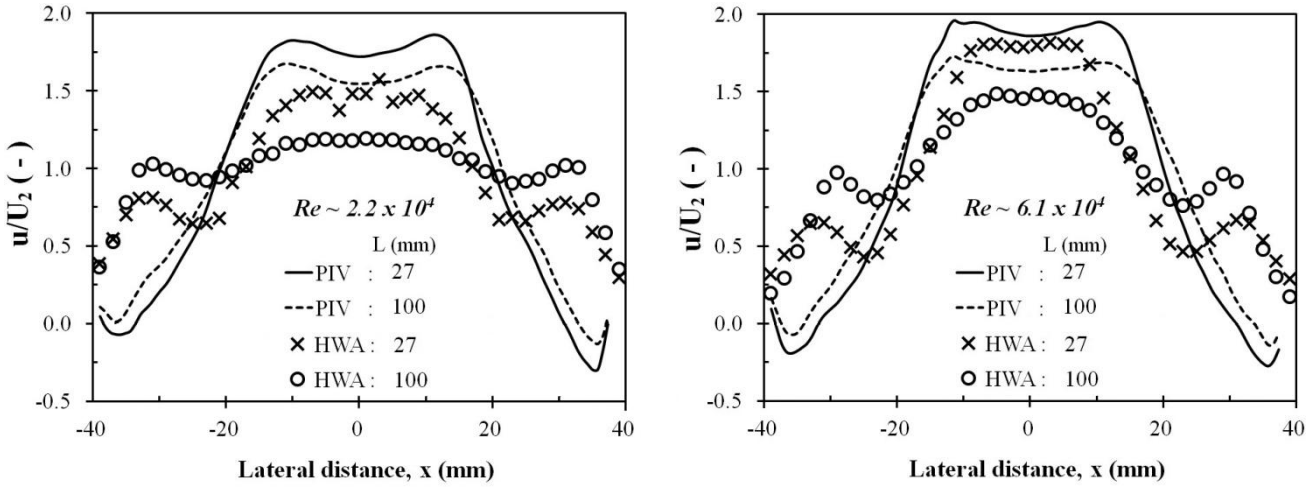

Fig. 6 Steady flow. Normalised axial velocity distributions 2.5 mm upstream (PIV) and 40 mm downstream (HWA); u axial velocity, U_2 mean velocity downstream of the monolith

Figure

Click here to download Figure: Figure 7 Int J of Heat and Fluid Flow 22 March 2012.docx

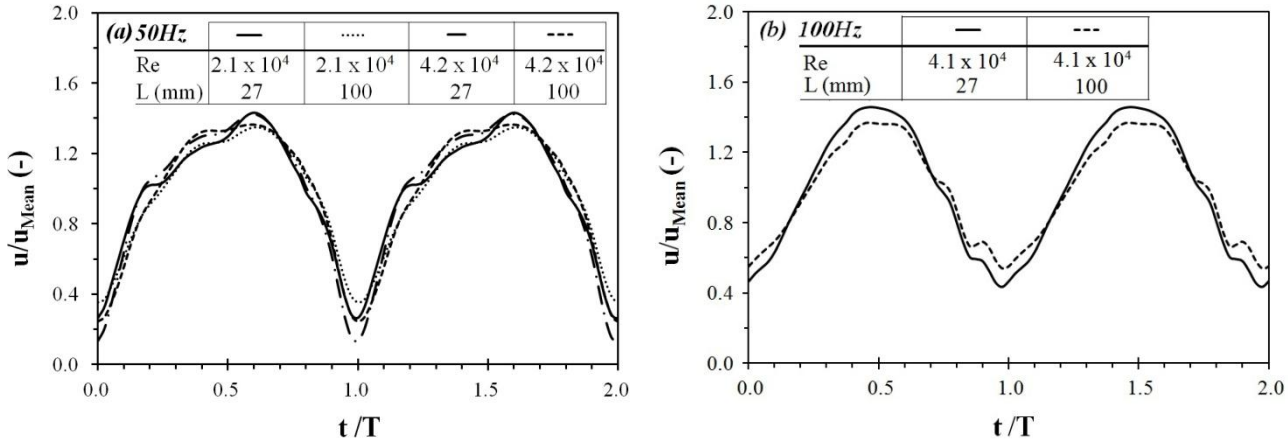

Fig. 7 Inlet pulse shapes observed at centre of the nozzle exit for (a) 100 Hz and (b) 50 Hz, t is the time, T pulse period, u phase-averaged velocity, u_{Mean} cycle-averaged velocity

Figure
Click here to download Figure: Figure 8 Int J of Heat and Fluid Flow 22 March 2012.docx

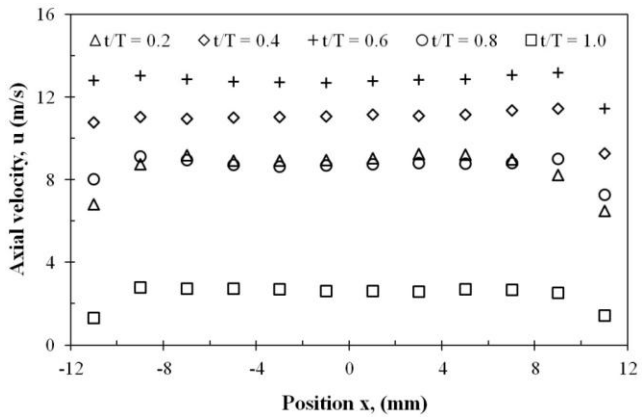

Fig. 8 Phase-averaged velocity profiles across centre of the nozzle exit (f = 50 Hz, Re = 2.1 x 10^4, L = 27 mm)

Figure

Click here to download Figure: Figure 9 Int J of Heat and Fluid Flow 22 March 2012.docx

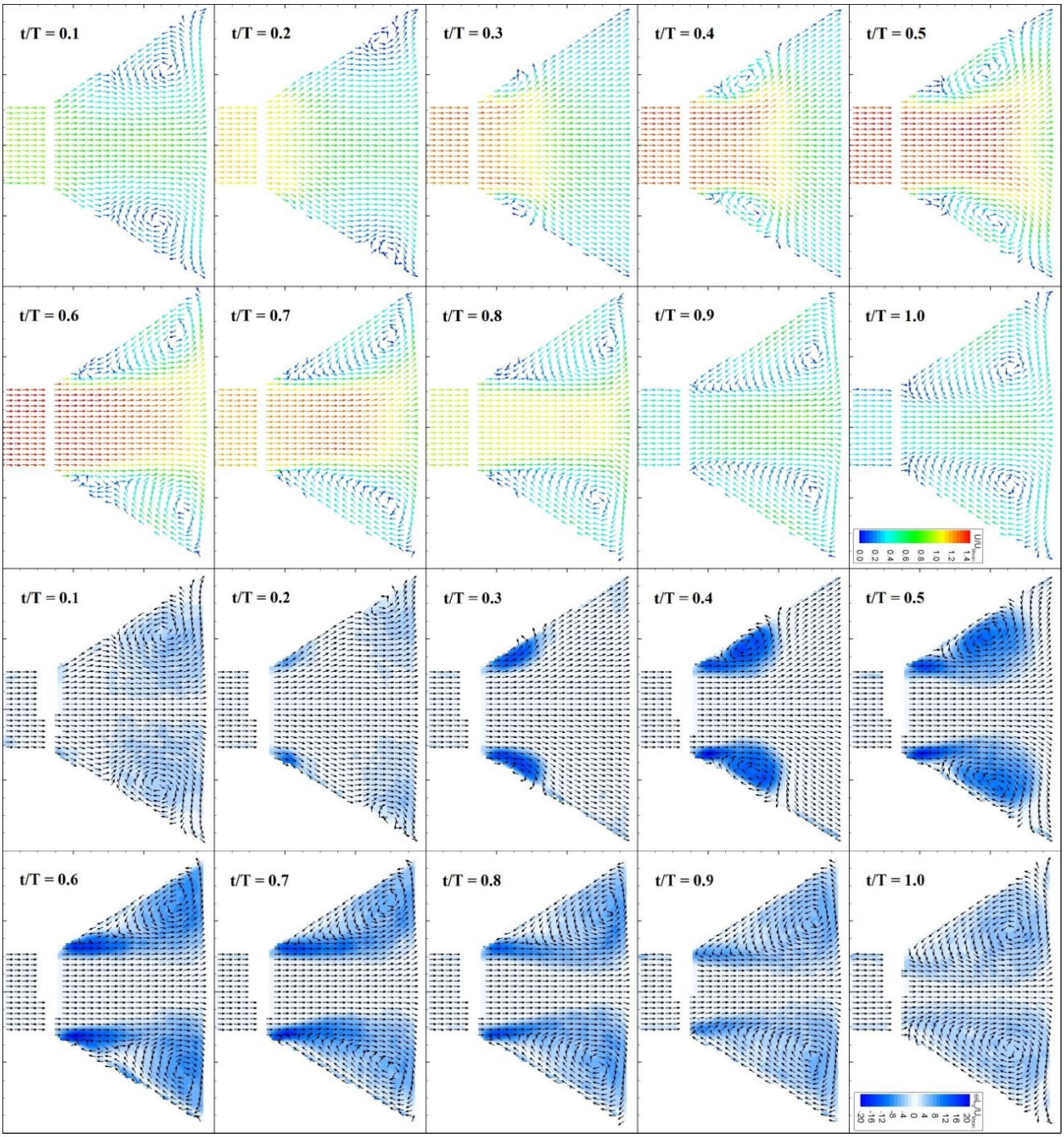

Fig. 9 Normalised phase-averaged velocity vector and vorticity fields for Case 3 at J = 6.8 (Re = 4.2x10^4, f =50 Hz, L = 27mm). Fields are normalised by the cycle-averaged mean inlet velocity

Figure
Click here to download Figure: Figure 10 Int J of Heat and Fluid Flow 22 March 2012.docx

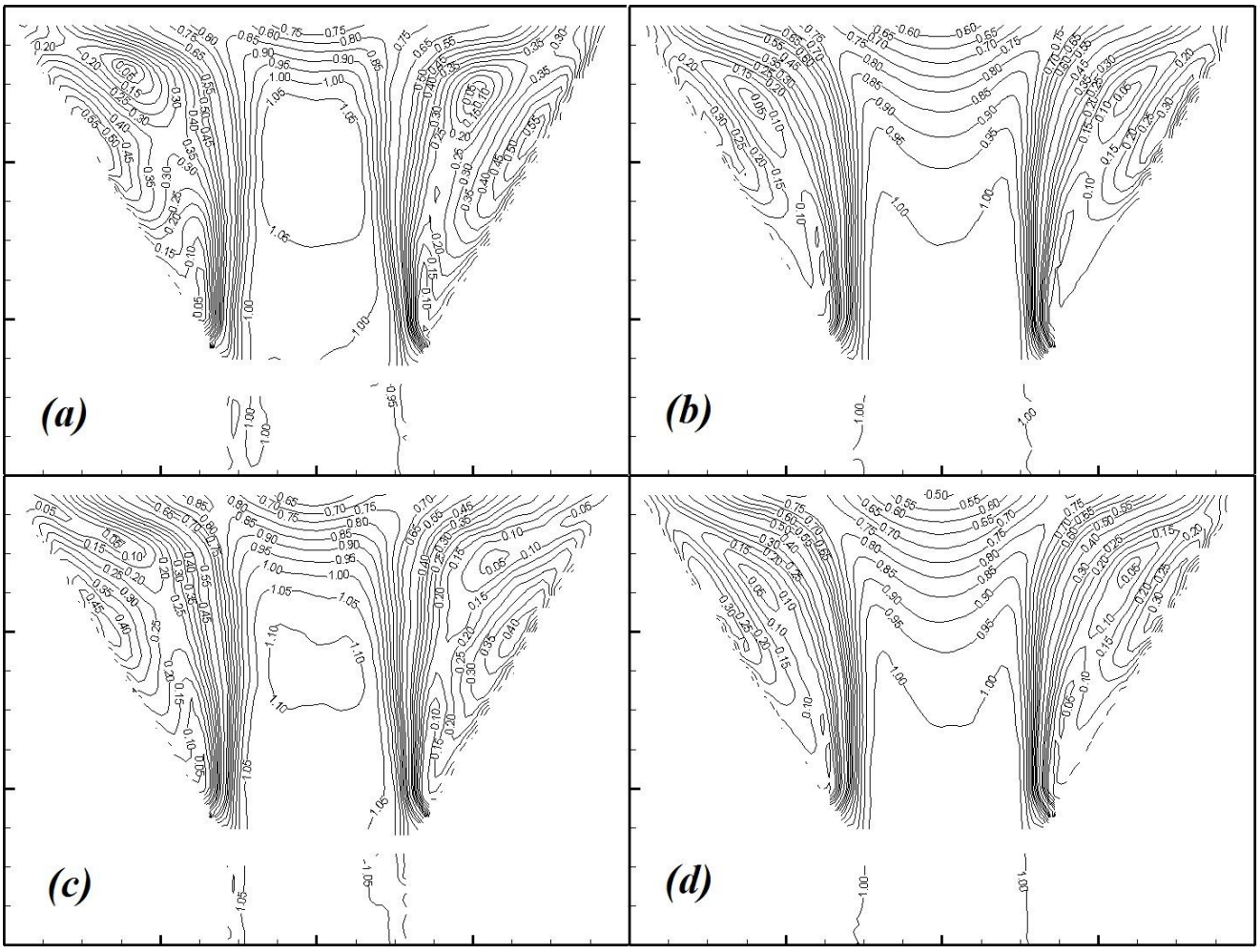

Fig. 10 Normalised velocity contours at Re ~ 4.2 x 10^4 (a) t/T = 0.8, Case (3), f = 50 Hz, L = 27 mm (b) Steady flow, L = 27 mm (c) t/T = 0.8, Case (4), f = 50 Hz, L = 100 mm (d) Steady flow, L = 100 mm. In (a) and (c) phase-averaged velocities are normalised by the cycle-averaged mean inlet velocity

Figure

Click here to download Figure: Figure 11 Int J of Heat and Fluid Flow 22 March 2012.docx

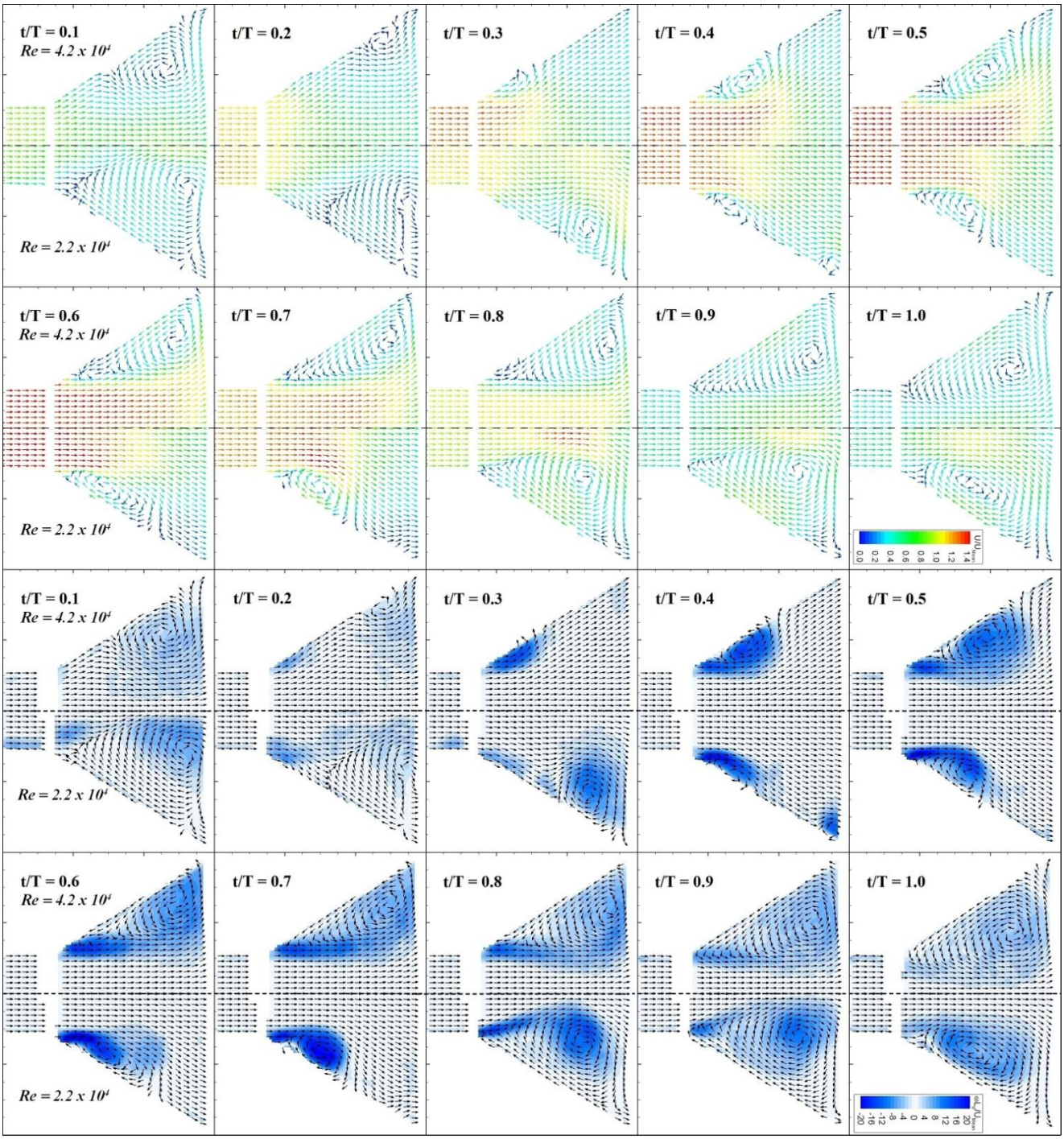

Fig.11 Normalised phased averaged velocity and vorticity fields for Case 1 (J = 3.6, Re = 2.2 x 10^4, 50 Hz) and Case 3 (J = 6.8, Re = 4.2 x 10^4, 50 Hz) for L = 27 mm. Fields are normalised by the cycle-averaged mean inlet velocity

Figure

Click here to download Figure: Figure 12 Int J of Heat and Fluid Flow 22 March 2012.docx

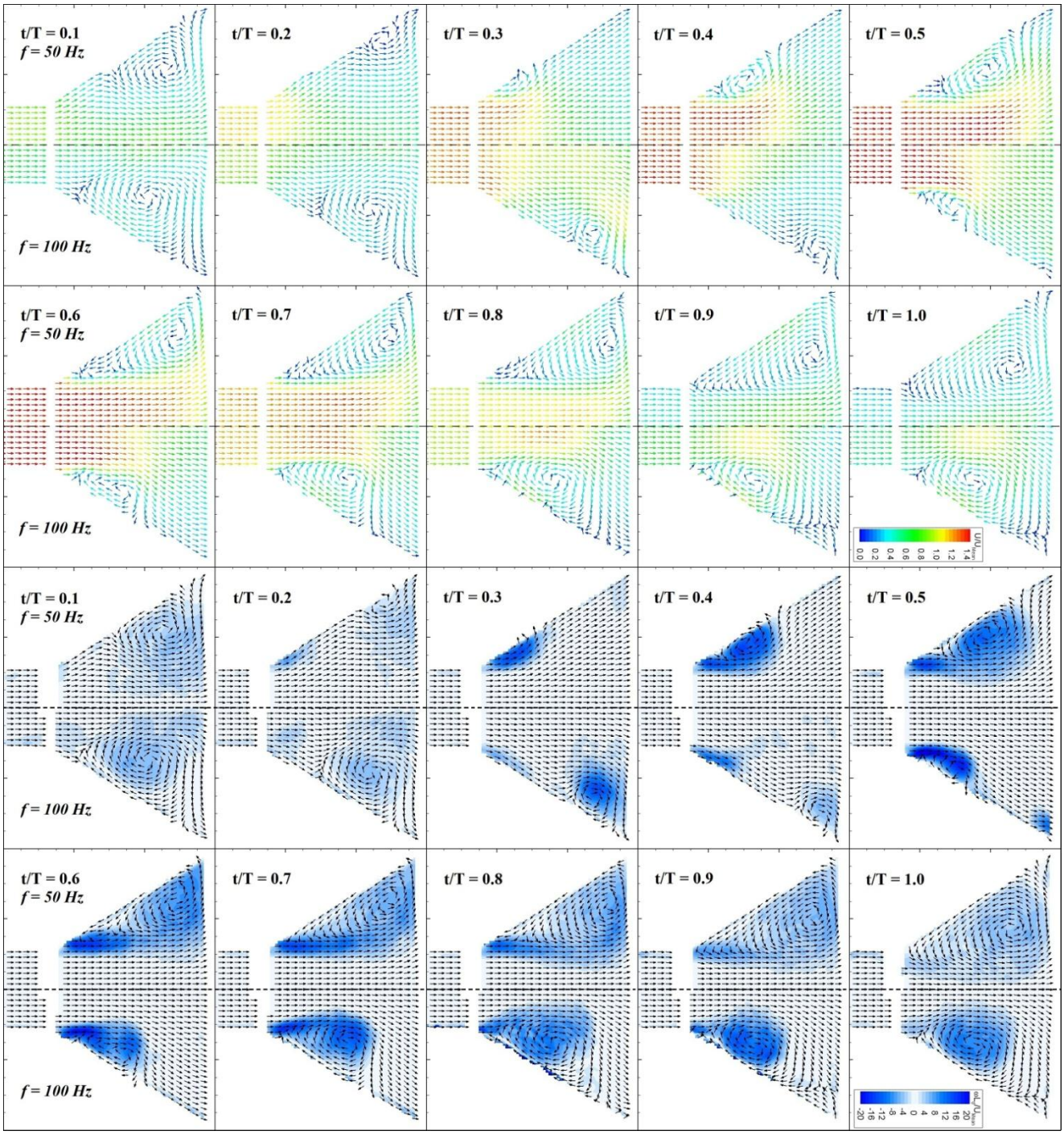

Fig. 12 Normalised phase-averaged velocity and vorticity fields for Case 3 (J = 6.8, Re = 4.2 x 10^4, 50 Hz) and Case 5 (J = 3.4, Re = 4.2 x 10^4, 100 Hz) for L = 27 mm. Fields are normalised by the cycle-averaged mean inlet velocity

Figure
Click here to download Figure: Figure 13 Int J of Heat and Fluid Flow 22 March 2012.docx

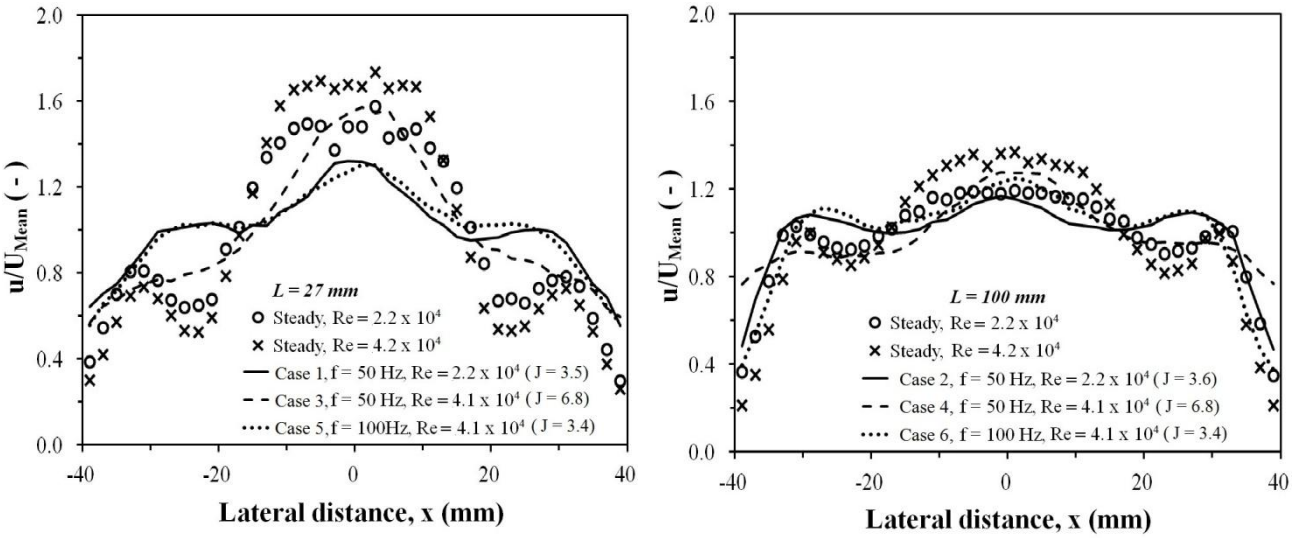

Fig. 13 Steady flow and cycle-averaged velocity profiles at the monolith exit. Velocities are normalised by the cycle-averaged mean velocity downstream of the monolith

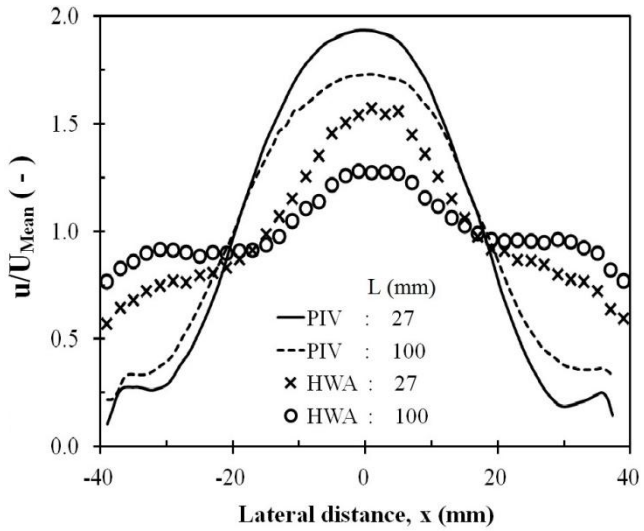

Fig. 14 Cycle-averaged velocity profiles measured 2.5 mm upstream (PIV) and 40 mm downstream (HWA) for Re ~ 4.2 x 10^4, f = 50 Hz, J = 6.8 for L = 27 mm and 100 mm (Cases 3 and 4). Velocities are normalised by the cycle-averaged mean velocity downstream of the monolith